Radiocarbon (2025), pp. 1–14
doi:10.1017/RDC.2024.133

CAMBRIDGE UNIVERSITY PRESS

RESEARCH ARTICLE

Investigating the impact of COVID-19 on the atmospheric ^{14}C trend and fossil carbon load at urban and background sites in Hungary

Balázs Áron Baráth[1,2,3], Tamás Varga[1,3], István Major[1,3], László Haszpra[1,4], Danny Vargas[5], Zoltán Barcza[6,7] and Mihály Molnár[1]

[1]International Radiocarbon AMS Competence and Training (INTERACT) Center, HUN-REN Institute for Nuclear Research, Debrecen, H-4026, Hungary, [2]Doctoral School of Environmental Sciences, ELTE Eötvös Loránd University, H-1117 Budapest, Hungary, [3]Isotoptech Ltd., Debrecen, H-4026, Hungary, [4]Institute of Earth Physics and Space Sciences, H-9400 Sopron, Hungary, [5]Isotope Climatology and Environmental Research Centre, HUN-REN Institute for Nuclear Research (ATOMKI), Bem tér 18/c, 4026 Debrecen, Hungary, [6]Department of Meteorology, ELTE Eötvös Loránd University, H-1117 Budapest, Hungary and [7]Faculty of Forestry and Wood Sciences, Czech University of Life Sciences Prague, 165 21 Prague, Czech Republic
Corresponding author: Balázs Áron Baráth; Email: barath.balazs@atomki.hu

Received: 31 January 2024; **Revised:** 01 August 2024; **Accepted:** 07 August 2024

Keywords: ^{14}C activity; accelerator mass spectrometry; CO_2; CO_2 fossil fraction time series; COVID-19; greenhouse gas; tree-ring

Abstract

The study analyses in situ CO_2 mole fraction, $^{14}CO_2$, and fossil based excess CO_2 mole fraction (C_{foss}) data at Hegyhátsál (HUN) rural monitoring station (Central Europe) supplemented by passive monitoring of ^{14}C content of tree-rings. Through the observed period (2014–2020) we focused on revealing trends in atmospheric CO_2 and ^{14}C levels, particularly during the year of the first COVID lockdown, in comparison to the preceding five years. In addition, monthly integrated samples of atmospheric CO_2 and tree-rings from the six years were subjected to ^{14}C analysis. The passive tree-ring measurements focuses on two major urban areas (Budapest and Debrecen) in Hungary, along with the rural monitoring site. Results show a steady increase in CO_2 levels at HUN between 2014 and 2020. The calculated fossil based excess CO_2 concentrations for the initial year of COVID are in good agreement with the previous five-year averages both at 115 m and 10 m elevations. These results also show seasonal variations of CO_2 mole fractions, peaking in winter and decreasing in summer. Tree-ring results from Debrecen show a good alignment with the results of the atmospheric monitoring station, and it does not show a significant fossil contribution in the urban background area during the vegetation periods. Tree-ring results from Budapest show a stronger fossil contribution compared to the Debrecen ones. Our atmospheric CO_2 results do not show a large decrease in fossil CO_2 atmospheric contribution during the first lockdown. We found that the use of this passive CO_2 monitoring technique can provide a valuable tool for investigating such differences.

Introduction

Carbon-containing gases in the atmosphere have a significant impact on our environment. The increased concentration of atmospheric carbon dioxide (CO_2) receives considerable attention not only from the side of the scientific community, but also from social and economic entities due to its crucial role in global climate change (Burgess et al. 2021; Heiskanen et al. 2022). Considering the extraordinary impact of COVID-19, a decrease occurred in global CO_2 emissions levels. Studies showed a notable

daily reduction by early April 2020 compared to 2019, attributed in large part to widespread government policies, especially in transportation (Le Quéré et al. 2020). Another study showed that by June 2020, the CO_2 levels had recovered rapidly in most countries except the United States, Brazil, and India. Notably, China's early May CO_2 emissions rose above 2019 levels (Liu et al. 2020). For the investigation of the impact of the lockdown on fossil CO_2 emissions in Mexico City, the study of Beramendi-Orosco et al. (2023) employed atmospheric radiocarbon concentrations as indicators. Analysis of $\Delta^{14}C$ values from January 2019 to December 2021 revealed a noteworthy shift in post-lockdown fossil CO_2 emissions, primarily attributed to reduced road traffic.

Several groups have used tree-ring measurements sucessfully to determine fossil CO_2 (Kontuľ et al. 2022; Lee et al. 2023; Zhou et al. 2022). Despite many studies being conducted regarding the topic, it is worth further exploring, especially considering the absence of such results in Hungary.

In 2020, Hungary as other nations, implemented stringent measures, including social distancing which were crucial in mitigating virus transmission but lead to an increase in car usage, especially in Budapest. In 2020, the National Toll Payment Services reported a minor decrease in truck toll revenue but a 4% increase in personal vehicle tolls, underscoring the persistence of car usage. This shift, coupled with gasoline and diesel sales, approximated or surpassed the pre-pandemic levels. This highlights the pandemic's impact on transportation habits and the challenges in reviving interest in public transportation which phenomenon was observable in large cities. However, a study in central Europe showed that pandemic-related restrictions led to a significant reduction (20%, in average) in the concentrations of air pollutants at all urban monitoring points. The significant reductions were associated with changes in transport-related pollutants, agricultural activities, and energy-related sources (Kertész et al. 2024).

When considering the challenges of using atmospheric CO_2 concentration observations as a sole proxy for assessing the pandemic's impacts, it is important to highlight the effect of natural variability from the inherently complex and dynamic global carbon cycle and meteorological conditions. This complexity introduces variability or "noise," that challenges the isolation of the pandemic's specific influences on atmospheric CO_2 concentrations in near-real time (Ballantyne et al. 2012; Friedlingstein et al. 2020; Le Quéré et al. 2020). Consequently, relying solely on atmospheric CO_2 fluctuations limits the unveiling of the pandemic lockdown's local-to-global scale impacts. Therefore, isotopic measurements such as radioactive carbon (radiocarbon, ^{14}C), that is present in atmospheric CO_2, can help to answer important questions. In addition, studying ring patterns of woody plants absorbing atmospheric CO_2 via photosynthesis, can provide a unique tool to gain information regarding the long-term fluctuation of this substantial isotope.

Radiocarbon plays a crucial role in global carbon cycle investigations and emission verification. It enables the estimation of regional fossil fuel CO_2 burden over highly populated areas, by using specific radioactivity measurements in atmospheric CO_2 or single tree-rings (expressed as $\Delta^{14}C$, according to the definition in Stuiver and Polach [1977; Trumbore 2009]). Comparing the $\Delta^{14}C$ values of respective CO_2, plant material, such as leaves or tree-ring samples, any depletion in the $^{14}C/^{12}C$ ratio at the polluted site relative to the background can be directly translated into fossil fuel CO_2 excess data (Graven et al. 2012; Levin et al. 1989, 2010; Meijer et al. 1996; Molnár et al. 2010a; Sharma et al. 2023; Svetlik et al. 2010; Zondervan and Meijer 1996). In the case of atmospheric CO_2, the resolution of the decreased fossil emission during the pandemic depends on the collecting period of samples, but for trees, only the vegetation period when the CO_2 uptake is active via photosynthesis. The aim of this research was to evaluate the effects of the initial Hungarian COVID-19 lockdown measures on atmospheric $^{14}CO_2$ levels in the two largest Hungarian cities, Budapest and Debrecen, by comparing the tree-ring data to the data of the regional background HUN station and the High Alpine Research Station Jungfraujoch (JFJ) background station located in Switzerland. Thus, our primary focus revolved around examining the effects of the first lockdown and its comparison to the preceding five years.

https://doi.org/10.1017/RDC.2024.133 Published online by Cambridge University Press

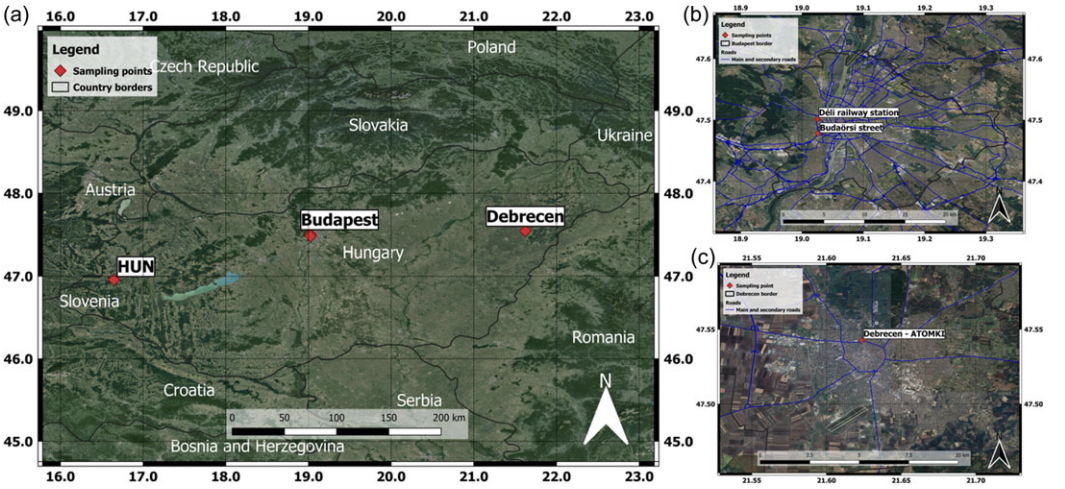

Figure 1. *Location of the atmospheric CO_2 and tree-ring sampling sites in Hungary (Figure 1.a.). At the HUN site, both tree-ring and atmospheric CO_2 samples were collected. In Budapest (Figure 1.b.), tree-ring samples were collected from two distinct busy junctions. In Debrecen (Figure 1.c.), tree-ring samples were collected in an urban background.*

Materials and methods

Study area and sampling procedure

Sampling was carried out at three locations (Figure 1.a.) in Hungary. The HUN regional background monitoring station of the Integrated Carbon Observation System (ICOS) is located in Western Hungary (46°57.359'N, 16°39.126'E.). The tower is surrounded by agricultural fields (mostly crops and fodder of annually changing types), pastures and small forests. The industrial and heavy transportation activity in the region is negligible. The closest habited area is the Hegyhátsál village (~ 150 inhabitants) situated 1 km to the northwest from the station. A detailed description of the HUN tower monitoring site can be found in several previous publications (Haszpra et al. 2005, 2008, 2012. At the station, the CO_2 mole fraction has been continuously monitored at four elevations (115, 82, 48 and 10 m above the ground) since 1994, using a Li-Cor (Model LI-7000) non-dispersive infrared gas analyzer (Model LI-7000) Haszpra et al. (2008), and lately by a Picarro G2310 CRDS analyzer. The overall uncertainty of the measurements is ±0.1 ppm. The HUN monitoring station is a member of the NOAA atmospheric monitoring network (Haszpra et al. 2008; Molnár et al. 2010a) and joined to the ICOS network in 2022 (HUN station). Continuous mole fraction measurements were supplemented by monthly integrated $^{14}CO_2$ air sampling from two elevations (115 and 10 m a.g.l.) in 2008, in cooperation with the Hertelendi Laboratory of Environmental Studies of Institute for Nuclear Research (HEKAL, ATOMKI, Molnár et al. 2010b). For this study, monthly integrated atmospheric $^{14}CO_2$ samples, supplemented with CO_2 mole fraction measurements, were collected from October 2014 to December 2020. This includes measurements of CO_2 mole fraction and $\Delta^{14}C$ at two distinct elevations (115 and 10 meters above ground level) at HUN (ICOS), and a tree-ring core sample originating from the close vicinity of the atmospheric sampling station. The data were studied from the aspect of temporal variation and altitudinal differences. The Past 4.03 software was used to remove the trend from the $\Delta^{14}C$ and CO_2 mole fraction time-series (Hammer et al. 2001).

Trajectory analysis was performed to quantify and visualize the region that influences the observed CO_2 mole fraction and its isotopic composition at the HUN tall tower site. For this purpose backward trajectories were calculated using 72 hours duration using the latest version of the HYSPLIT model (v5.3.0, Draxler and Hess 1998; Stein et al. 2015). Due to data availability constraints and consistency, we used the NOAA FNL meteorological data with $1° \times 1°$ horizontal resolution. The initial height for the

https://doi.org/10.1017/RDC.2024.133 Published online by Cambridge University Press

trajectories was set to 115 m, and simulations were initiated with 12 hours frequency for the entire 2014–2020 time period. The backward trajectories were separated to cover the heating period (from October to March), and the vegetation season (April to September), separately, for each year. For the quantification of the source regions, a regular grid was defined first with 0.5° × 0.5° degree horizontal resolution. Then, using the trajectory center points and the grid geometry it was counted how many times an individual trajectory crossed a given grid cell.

In a regional context, CO_2 mole fraction data of the free tropospheric background station of JFJ (46° 33'N, 7°59'E, 3450 m a.s.l., ~660 km west of HUN station) was considered as a background for the study period. The CO_2 mole fraction at the JFJ station has been continuously measured by the University of Bern, using a S710 UNOR type non-dispersive infrared gas analyzer. Monitoring of $^{14}CO_2$ was launched in 1986 by the University of Heidelberg (Levin et al. 2013). Since 2018, the University of Bern has performed the measurements as part of the ICOS (Hammer et al. 2017). The overall uncertainty of the measurement is ±0.1 ppm (Sturm, 2005).

The second sampling site was in Budapest (Figure 1), Hungary's capital, situated in the Carpathian Basin along the Danube River. According to the Hungarian National Statistical Office, the current metropolitan area population of Budapest is reported to be 1.7 million. Spanning around 525 km^2, Budapest displays an average population density surpassing 3200 people/km^2, with notable variations observed among its 23 districts. Each district presents distinct yet highly urbanized land use and land cover patterns. The Buda side (west of the Danube) stands out for its abundance of green areas (Buzási 2022). Despite being characterized by extensive vehicular and human activity, the city experienced a "state of emergency" from March 11 to June 18, 2020, in response to the COVID-19 pandemic (Kovalcsik et al. 2021). During the lockdown in Budapest, exceptions were made for freight traffic crossing the border and passenger traveled due to business and economic reasons (MANFQ, 2021). Both of our sampling points were located in Buda: one next to Déli railway station (47°30'07.2"N 19° 01'29.0"E), and the second on Budaörsi Road (47°28'41.2"N 19°01'32.1"E). Both sampling sites are characterized by a bustling urban environment, with a mix of vehicular activities contributing to the local atmosphere (Figure 1b).

The third sampling location lies in the Eastern part of Hungary. Debrecen (Figure 1.c.), the second-largest city in the country, boasts a population of 202 thousand inhabitants with 433 people/km^2 (Hungarian Central Statistical Office, 2023). The main contributors to pollution in the area are urban vehicular traffic and the surrounding agricultural regions. Despite the absence of significant industrial activities in the area, the city is currently experiencing an industrial development, characterized by the construction of major facilities. The emissions from tourism are not significant. Previously, atmospheric $^{14}CO_2$ sampling and plant measurements have been studied in Debrecen at ATOMKI, for determination of the fossil CO_2 excess relative to the HUN and the JFJ background sites (Major et al. 2018; Molnár et al. 2010b; Varga et al. 2019a). For this study, a tree-ring core sample was collected in the backyard of ATOMKI (47°32'33.5"N, 21°37'25.2"E), which is located in an urban background area in Debrecen. It is important to note that the effect of the nuclear bomb-tests in the Great Forest (located next to Debrecen) was already studied for the atmospheric ^{14}C level (Hertelendi and Csongor 1983).

Processing of the atmospheric $^{14}CO_2$ samples

At the HUN station, two atmospheric $^{14}CO_2$ sampling units developed by ATOMKI have been installed to collect monthly integrated samples for ^{14}C measurements (Molnár et al. 2010b). The inlets of the $^{14}CO_2$ samplers at the HUN station are connected to the exhaust lines of the CO_2 analyzer in use, thus the sampling of CO_2 does not interfere with the CO_2 monitoring process. CO_2 is trapped in bubblers filled with a solution of 500 mL 3M NaOH. The 10 L h_{-1} (STP) flow rate is controlled by a specific control unit. Sampling is scheduled for 4–5 week cycles. A detailed description of the sampling device is given by Major et al. 2018. In the preparation process, 2 mL sulphuric acid were added to 2 mL $NaHCO_3$ exposed solution, and the extracted CO_2 was purified in a dedicated vacuum line (Molnár et al. 2010b).

https://doi.org/10.1017/RDC.2024.133 Published online by Cambridge University Press

Preparation of the tree-ring samples

The tree-ring core sample were taken using a Haglöf Mora 5.15/400 mm increment borer. The increment cores were mounted with the direction of vessels vertically aligned and air-dried in the laboratory. Then, the cores were consecutively sanded until 600 grit and scanned in an Epson Perfection V600 to 2400 dpi optical resolution. Tree-ring width was measured using the image analysis software CooRecorder following a visual cross-dating of samples to corroborate the synchronicity of measurements, detect errors or missing rings and assign a calendar year to each ring (Maxwell et al. 2021; Stokes and Smiley 1968). The tree-rings from 2014 to 2020 were selected from cores and visually separated using a EuromexNexius Zoom stereo microscope and a scalpel. The stable and most accurate ^{14}C measurements can be performed on the cellulose fraction of wood samples. Thus, the cellulose was prepared from the separated tree-rings by the standard BABAB (basic-acid-basic-acid-bleaching) cellulose preparation method (Němec et al. 2010; Varga et al. 2019a). Then, the purified, dry cellulose was combusted with MnO_2 reagent as an oxidizing agent to convert the carbon content of the sample to CO_2 at 550ºC, 12 hr (Janovics et al. 2018; Varga et al. 2019b). The released gas was purified in a vacuum line described in Janovics et al. (2018).

Graphitization and AMS ^{14}C measurement of the atmospheric and tree-ring samples

The pure CO_2 extracted from the atmospheric CO_2 and tree-ring samples were then graphitized using the sealed tube graphitization method described in Rinyu et al. (2013). The AMS ^{14}C measurement of graphite targets was performed in the INTERACT Centre, Debrecen, Hungary, by a Mini Carbon Dating system (MICADAS) type accelerator mass spectrometer (Molnár et al. 2013; Wacker et al. 2010). The overall uncertainty of the ^{14}C measurements (1σ) was around ±3‰. The result of the samples is reported in $\Delta^{14}C$ units corrected for radioactive decay of ^{14}C and fractionation of the stable ^{13}C isotope (Stuiver and Polach 1977).

Quantification of the fossil and modern excess CO_2

By analysing the $^{14}C/^{12}C$ ratio and the CO_2 mole fraction, the contribution of fossil CO_2 can be determined at the study site compared to a reference site.

Long-term atmospheric $^{14}CO_2$ observations allow us to investigate the temporal variation of the fossil fuel CO_2 excess. According to the model proposed by Levin et al. (1989, 2003), the measured CO_2 mole fraction (c_{meas}) at a given location consists is constituted three different components: a continental background component (c_{bg}), a regional biospheric component (c_{bio}) and a fossil fuel component (c_{foss}). To assess the excess CO_2 derived from fossil fuels, a mass balance equation was used that includes the measured CO_2 mole fraction and $\Delta^{14}C$ values:

$$c_{meas} \times \left(\Delta^{14}C_{meas} + 1000\right) = C_{bg} \times \left(\Delta^{14}C_{bg} + 1000\right) + C_{foss} \times \left(\Delta^{14}C_{foss} + 1000\right) + C_{bio} \times \left(\Delta^{14}C_{bio} + 1000\right) \quad (1)$$

Here, c_{meas} is the mole fraction of CO_2 at the observed site, c_{bg} is the mole fraction of background in the free troposphere, c_{foss} is the fossil fuel and c_{bio} is the biogenic component. $\Delta^{14}C_{meas}$, $\Delta^{14}C_{bg}$, $\Delta^{14}C_{bio}$ and $\Delta^{14}C_{foss}$ represent the deviation of $^{14}C/^{12}C$ ratios from "modern", defined as 95% of the standard activity of NBS oxalic acid (SRM4990B) and corrected for fractionation and radioactive decay. A detailed description can be found in Levin et al. 1989, 2003.

In our study, for this calculation, measured values from JFJ as $\Delta^{14}C$ background were used. In equation (1), the fossil fuel term was set to zero since $\Delta^{14}C_{foss} = -1000‰$, indicating that the total ^{14}C content of these materials has decayed.

https://doi.org/10.1017/RDC.2024.133 Published online by Cambridge University Press

To compare the measured CO_2 mole fractions at 115 m and 10 m elevations of the HUN station relative to JFJ, the difference (δc) was calculated as follows:

$$\delta C = C_{meas} - C_{bg} \tag{2}$$

where c_{meas} represents the CO_2 mole fractions at the specified elevations of HUN, and c_{bg} represents those at JFJ.

By rearranging equation (1), the following formula is obtained:

$$c_{foss} = c_{meas} \times \frac{\Delta^{14}C_{bg} - \Delta^{14}C_{meas}}{\Delta^{14}C_{bg} + 1000} \tag{3}$$

This is suitable for calculating the fossil fuel component.

Atmospheric CO_2 mole fraction and $\Delta^{14}C$ data were utilized from the HUN and JFJ stations, considering the latter as the background reference. For JFJ background site, we lacked precise information on modern and fossil contributions to atmospheric CO_2. In this study it was assumed to be predominantly free from direct and significant anthropogenic influences.

$$C_{mod} = \delta C - C_{foss} \tag{4}$$

Results and discussion

Seasonal variations in the atmospheric CO_2 mole fraction at HUN between 2014–2020

During the investigated six-year-long period (2014–2020), the yearly mean of CO_2 mole fraction at the 115 and 10 m elevations of the HUN station increased from 405 to 420 ppm and from 414 to 430 ppm (Figure 2). The mean values for the whole observation period from September 2014 to December 2020 are 414.4 ppm (at 115 m) and 429.9 ppm (at 10 m) at the two levels, respectively. All data used in the study can be found in the Supplementary material S1 file.

The maximum annual average of CO_2 mode fraction values at HUN were recorded in November/December and the minimum values in May/June which aligns with the Major et al. (2018) study, that investigated the previous six years (2008–2014) and with the typical seasonality of atmospheric CO_2. The observed atmospheric carbon dioxide mole fraction exhibits seasonal variations. Comparing the average interannual changes from one year to another the biggest increase was observed between 2014 to 2015 at the elevation of HUN 115 m it was +3.6 ppm/yr. Interestingly, at the height of 10 m it was observed between 2016 and 2017 with +4.5 ppm. The 10 m level represents a more localised environment, while the 115 m gives a broader, regional picture. The highest annual step in JFJ station was observed between 2014 and 2015 when the yearly average CO_2 mole fraction values increased from 401.1 ppm to 405.4 ppm.

The observed rate of increase averaged around 2.4 ppm per year at both the HUN-115 m and JFJ sites between 2014 and 2020. In comparison, the rate was slightly higher, reaching 2.6 ppm per year at the HUN-10 m level. These findings highlight the consistent upward trend in carbon-dioxide levels over the specified periods at the respective monitoring locations. Comparing the average annual increase to the first COVID-19 lockdown in 2020, a 2.9 ppm increase was observed at 115 meters, and a 3.3 ppm increase at 10 meters. However, at the JFJ station, the increase was slightly lower (2.2 ppm). The increase in CO_2 concentration was respectively higher in the first lockdown period.

The heating period in Hungary typically spans from October to March, while the vegetation season occurs from April to September. Higher monthly concentrations, specifically 420.2 (115 m) and 426.3 ppm (10 m), are detectable during the winter heating periods. In contrast, the vegetation periods are marked by comparatively lower values, specifically 407.3 (115 m) and 420.3 ppm (10 m). This seasonal fluctuation in carbon dioxide levels is indicative of natural patterns influenced by heating demand and

https://doi.org/10.1017/RDC.2024.133 Published online by Cambridge University Press

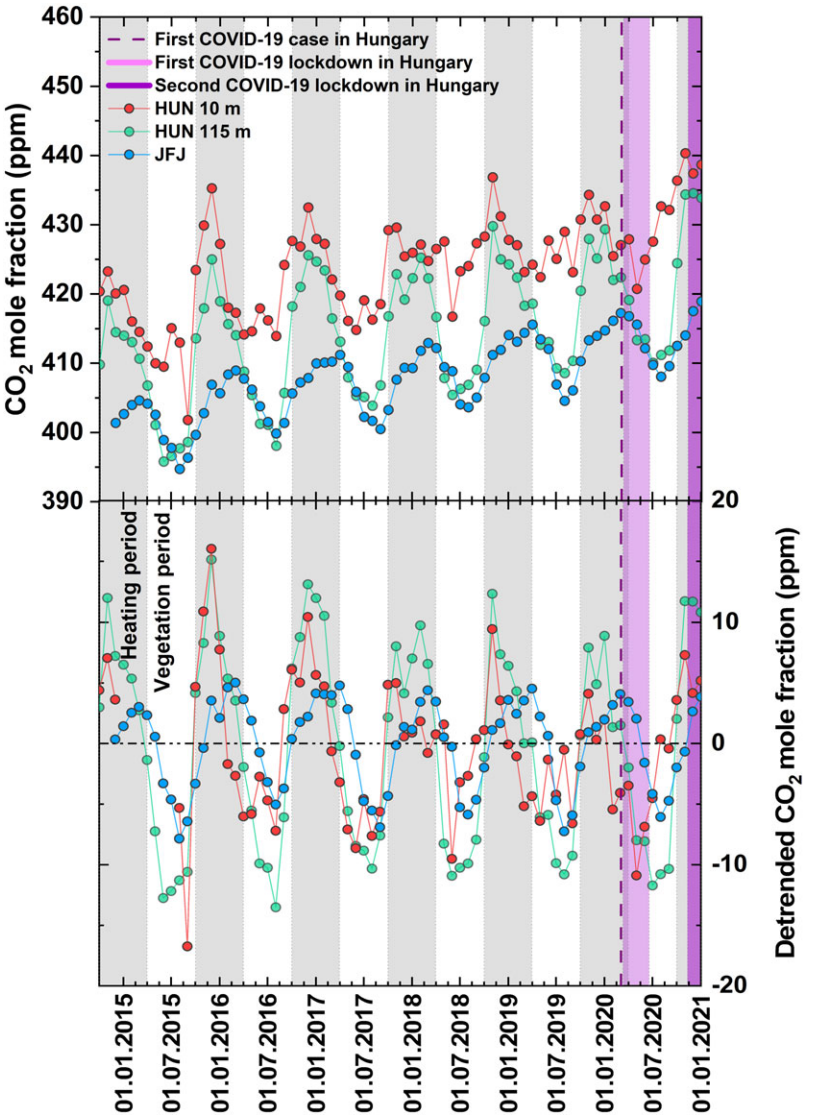

Figure 2. *Seasonal variation of monthly mean CO_2 mole fraction and the detrended curves at HUN and JFJ between October 2014 and December 2020.*

vegetation activity. If we examine the yearly CO_2 average growth of the growing season and the winter heating period, we can find that there is no significant difference in the first year of the Hungarian COVID-19 lockdown compared to the previous 5 years (2015–2019).

The peak-to-peak differences of the detrended data at JFJ vary from 10 to 12 ppm, while it ranges from 18 to 29 ppm and from 11 to 33 ppm at the 115 m and 10 m elevations at the HUN station, respectively. The lower CO_2 mole fraction values represent the summer months when vertical mixing is dominant and the CO_2 uptake by agricultural and natural vegetation is significant. Higher peaks in CO_2 were mainly observed in winter. These maximums possibly due to the limited vertical mixing, lack of CO_2 uptake through photosynthesis and the increased anthropogenic emissions that come from nearby cities. No significant changes can be observed in the detrended CO_2 mole fraction data due to COVID-19 pandemic in 2020.

https://doi.org/10.1017/RDC.2024.133 Published online by Cambridge University Press

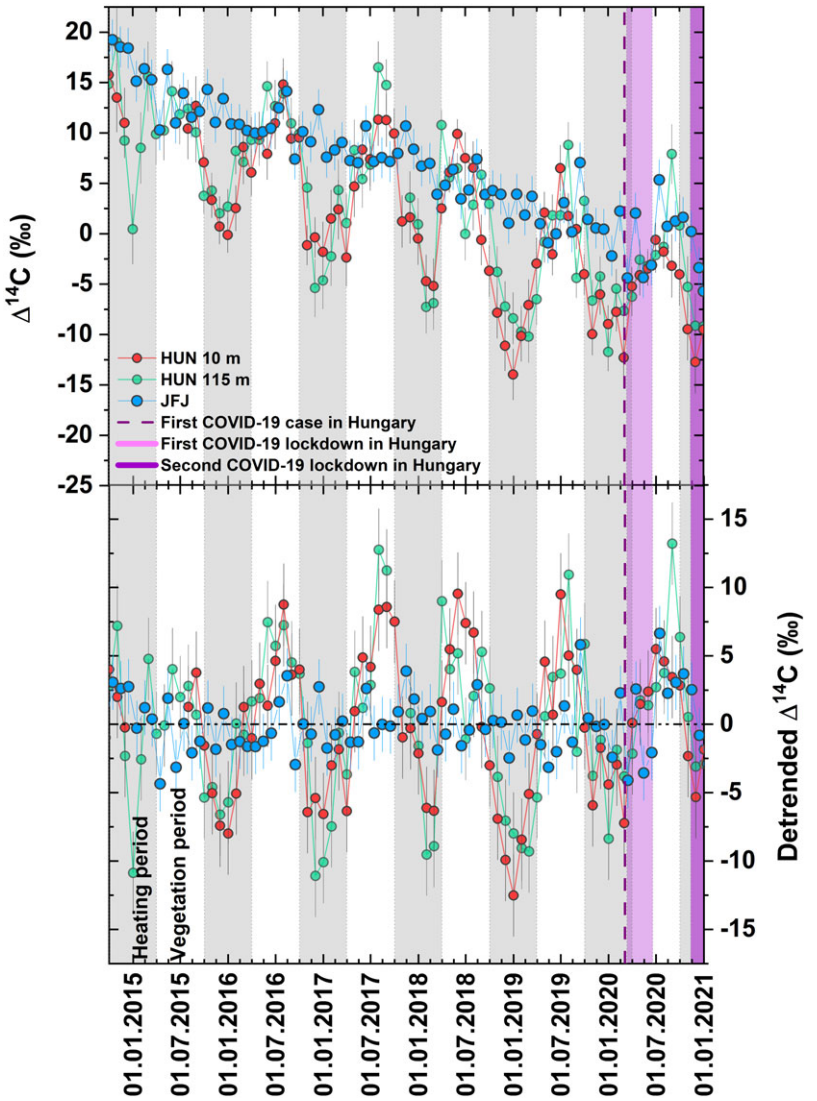

Figure 3. *Seasonal variation of monthly mean $\Delta^{14}C$ of CO_2 at HUN between October 2014 and August 2020.*

Long-term seasonal variation of the atmospheric $\Delta^{14}C$ at HUN

The $\Delta^{14}C$ values of atmospheric CO_2 are continuously decreasing at both levels of the regional background station, dropping below 0‰ ($\Delta^{14}C$) level after 2016. This trend can be attributed to the continuous decreasing trend of global $\Delta^{14}C$ and the release of huge amounts of fossil fuel (^{14}C free) CO_2 into the atmosphere (Figure 3). This observation also aligns with the research of Major et al. (2018) from the previous period (2008–2014).

During the observation period, the annual mean of $\Delta^{14}C$ values measured at the free tropospheric station JFJ decreased from 19 to –0.7‰ with an average decline of 2.8‰ yr^{-1}. For the same period, the annual mean $\Delta^{14}C$ values at the 115 and 10 m elevations decreased from 9.2 to –3.3‰ and from 6.9 to –4.6‰. The mean $\Delta^{14}C$ values of the two levels calculated for the whole period were 2.8 and 1.6‰. For the heating periods, relatively similar mean values of 0.5 and 0.3‰ were obtained while the vegetation periods were characterised by the higher means of 6.1 and 5.2‰, respectively. It is important to mention

https://doi.org/10.1017/RDC.2024.133 Published online by Cambridge University Press

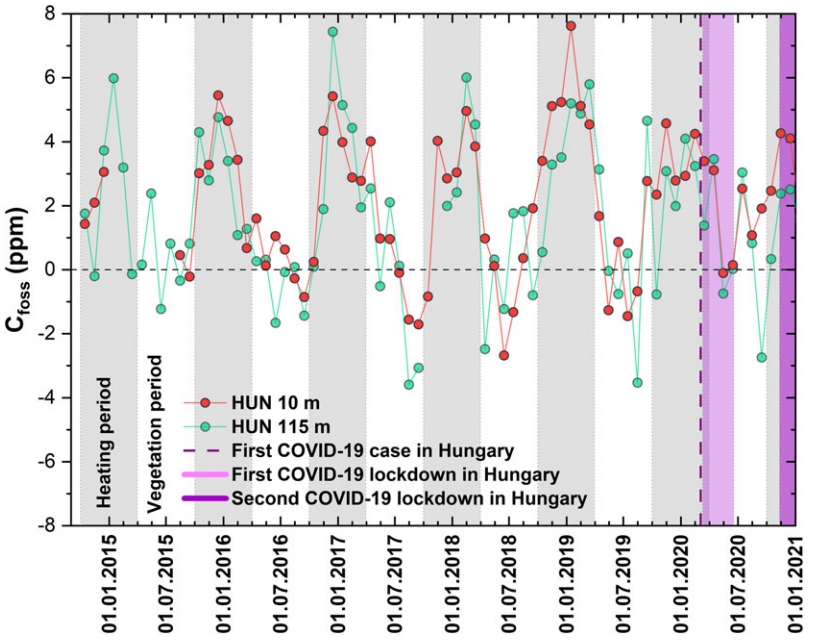

Figure 4. *The calculated fossil CO_2 excess values at the 115 and 10 m elevation of HUN, relative to JFJ.*

that atmospheric $\Delta^{14}CO_2$ is lower in winter, this can possibly indicate an increased emphasis on CO_2 depletion during this time of the year due to the increased fossil CO_2 emission. This observation also aligns with the previous measurements at HUN (Major et al. 2018).

Atmospheric fossil and modern CO_2 seasonal variation at HUN, relative to JFJ

Based on the absolute CO_2 mole fraction and $\Delta^{14}C$ data, we can calculate the CO_2 excess of fossil fuels at the two elevations of the HUN station compared to a background site (JFJ) (Figure 4). The JFJ is considered representative of the free troposphere of the mid-latitudes of the Northern Hemisphere, which is generally considered to be free of direct anthropogenic contributions. However, it is essential to acknowledge that even at this high-altitude position in the heart of Europe, it is still influenced by the surrounding continental fossil sources, especially in summer (Levin et al. 2008). In addition, Turnbull et al. (2015) showed that whether using a free tropospheric or continental station as a background for calculations, the excess CO_2 from fossil fuels effectively reflects not only the CO_2 emissions of the observation area, but also the CO_2 emissions of the wider continental region, which includes other urban areas and regional emission sources. Considering that JFJ is classified as a continental background station (while HUN is a rural one), this statement also holds true for our results (Major et al. 2018).

The calculated fossil CO_2 surplus values at 115 m and 10 m in HUN are shown in Figure 4. The annual mean of fossil fuel CO_2 excess was 1.6 ppm (115 m) and 1.9 ppm (10 m). Higher values were observed at the lower measurement point (10 m), but the average of the results was not significantly different. The annual maximum and minimum of the differences ranges between 5 and 12 ppm at 115 m and 5 and 10 ppm at 10 m. Our findings show that the minimum occurs during summer and the maximum during winter. All these results are in good agreement with the results of (Major et al. 2018).

As stated above, seasonal variability in the CO_2 difference between HUN and JFJ altitudes is strongly driven by seasonality in the daily planetary boundary layer height. Given the rural characteristics of the site, our back trajectory analyses indicate that the observed excess does not come exclusively from local fossil sources, such as domestic heating or transport rather, it represents a

https://doi.org/10.1017/RDC.2024.133 Published online by Cambridge University Press

cumulative effect from a larger geographical area, including bigger cities or capitals as Budapest or Vienna (Major et al. 2018). The occurrence of negative values of C_{foss} during the vegetation period, such as –3.5 or –4 ppm, can be attributed to the photosynthetic activity of local vegetation. During the vegetation period, plants absorb significant amounts of CO_2 for photosynthesis, this can lead to a noticeable reduction in the local atmospheric CO_2 concentrations. Another reason could be that in some cases, CO_2 levels measured at JFJ can be higher than those at HUN, leading to a negative C_{foss} and CO_2 excess (see equation 3).

The first COVID-19 lockdown in Hungary started on 11 March 2020. Several measures were subsequently implemented, including the closure of universities, border closures. Out of the five COVID waves in Hungary, the first lockdown was the strictest. Following an increased easing of the restrictions, the state of emergency ended on 18 June 2020, effectively concluding the first lockdown. Therefore, C_{foss} results should be examined from March to June for the first lockdown. We found that the average for the selected period at 115 m in 2020 was 1.03 ± 0.92 ppm, while the average for the previous 5 years was 0.84 ± 0.47 ppm ($\sigma = 2.12$). We conducted an independent two-sample t-test with unequal variances (Welch's t-test) comparing the 2020 data to the combined data from the previous five years, resulting in a p-value of 0.86, indicating no statistically significant difference between the two periods. A similar result can be observed for the 10 m height, as the average in the study was 1.63 ± 0.94 ppm (2020), while the average for the 4 years preceding period was 1.88 ± 0.47 ppm ($\sigma = 1.88$), with a p-vaue of 0.76, indicating no statistically significant difference between the two periods. The second lockdown started in November when the government imposed an 8 p.m. to 5 a.m. curfew. In the first two months of the lockdown no significant changes were detected in C_{foss} results. Since HUN station is in a rural area, it is mostly influenced by regional and global atmospheric transport rather than local anthropogenic emissions. During the lockdown, reductions in fossil fuel use (such as decreased vehicular traffic and industrial activity) would have had a more powerful impact in urban centers where such activities are concentrated. In rural areas, the baseline levels of C_{foss} are low, and the reduction in local fossil fuel emissions might not be sufficient to produce a noticeable change.

Back trajectory analyses

Due to the observed large differences between the vicinity of the tower and more distant areas, the logarithm of the crossover events was visualized in the form of annual maps (Figure 5). As close to the HUN site the frequency increased significantly, the high crossover numbers were truncated, so in the final maps the darkest shade might indicate larger numbers that can be calculated from the legend (where the latter provides logarithm of events with base 10).

The maps indicate that large geographical areas are affecting the chemical and isotopic composition of air masses that arrive at the tall tower site. These findings are consistent with those found by Gloor et al. (2001). The trajectory analysis shows that the pattern for the year 2020 does not differ from other years.

Tree-ring results at urban and background sites in Hungary

The analysis of HUN tree-ring section exhibited a correlation with results from the JFJ background station, signifying a consistent trend (Figure 6). For the tree-ring from Debrecen, we observed only minimal deviations. The average difference compared to the ^{14}C results of HUN is: –2.0‰, indicating a negligible presence of fossil loading during the vegetation period this aligns with the finding in Molnár et al. 2010a. In contrast, the Budapest results displayed more pronounced differences (average of Budaörsi Road was –8.3‰; average of Déli Railway station was –8.6‰), at both measurement points.

These findings are intriguing as the air of Budapest has not been analyzed using this method before. While the Déli railway station showed a notable increase in fossil load over 2020, Budaörsi Road indicated a state of stagnation. The results show that although stagnation was observed at the sampling

https://doi.org/10.1017/RDC.2024.133 Published online by Cambridge University Press

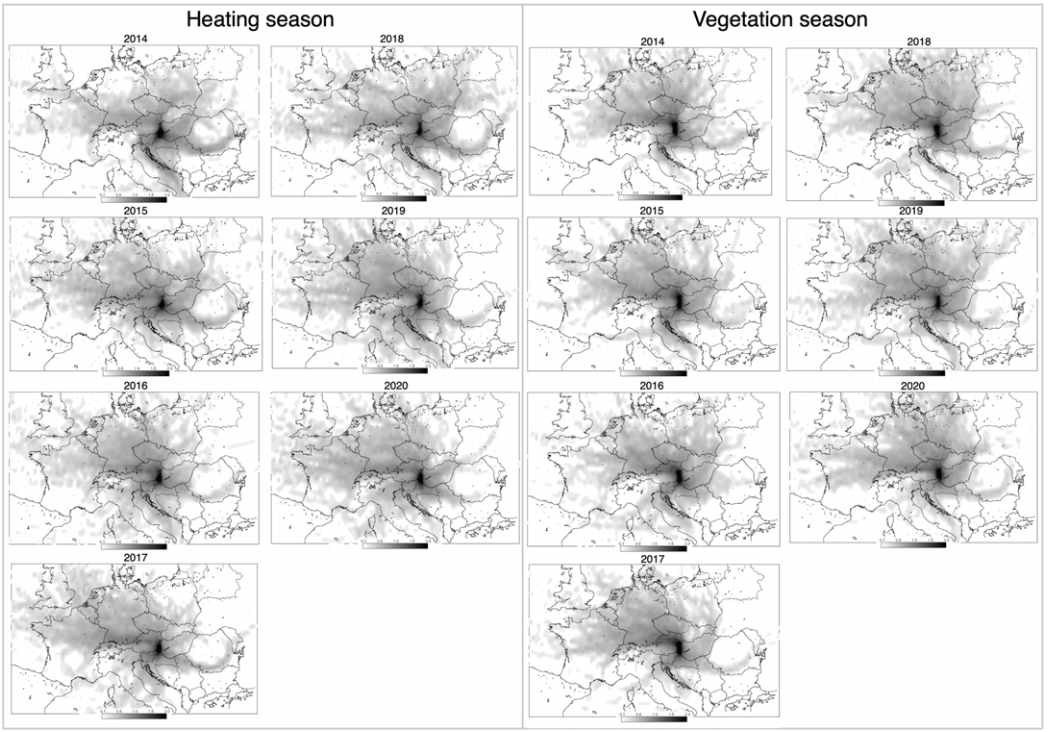

Figure 5. *Back trajectory analysis of the HUN monitoring station on an annual resolution, considering the heating and vegetation periods separately. For better visualization, we used a 10-logarithmic scale.*

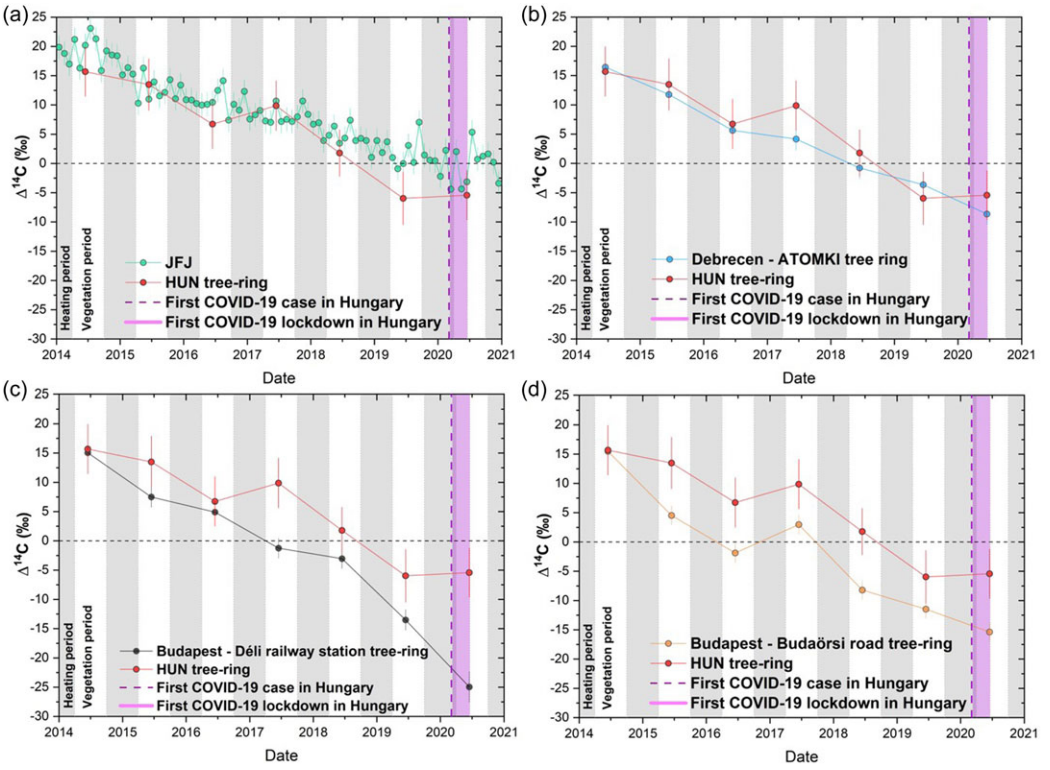

Figure 6. *Tree-ring ^{14}C results from HUN, Debrecen, and Budapest.*

https://doi.org/10.1017/RDC.2024.133 Published online by Cambridge University Press

point of Budaörsi road, which is a busy but outlying area of Budapest, an increase was observed in the city centre (Déli railway station), where vehicle traffic is more concentrated. The higher traffic may be due to the fact that during the pandemic, many people preferred not to use public transport but rather traveled by car (Varga et al. 2019a, 2019b). The results from the sampling sites suggest that the effect of COVID is not explicit. It is possible that local effects can be observed, which may even vary within cities. Our monitoring technique (tree-ring based) provides a good tool to examine such variation. Despite these variations, the conclusive findings suggest that the tree samples fail to show noticeable signs of the first but most significant COVID lockdown's impact, and a discernible reduction in fossil loading remains elusive.

Conclusions

Focusing on Hungary and emphasising urban areas (Budapest and Debrecen) and the regional background station at HUN, the research examines the first year of the Hungarian COVID-19 lockdown (2020) and the preceding five years. This study estimates seasonal variation of atmospheric CO_2 mole fraction and $\Delta^{14}C$ at two elevations of ICOS HUN station. The measured values were used to produce fossil and modern CO_2 time series compared to JFJ for the period 2015–2020. The average annual CO_2 molar fraction increased approximately by 15 ppm over the examined six years at both altitudes of HUN. These results follow the global CO_2 increase trend. Compared to the increase in the previous 6 years (observed between 2008–2014 by (Major et al. 2018), during the period under review, the CO_2 mole fraction increased by more than 4 ppm. We studied CO_2 mole fraction at two elevation and found seasonality in CO_2 mole fraction and $\Delta^{14}C$ results. The CO_2 mole fraction values were higher in the heating period and lower in the vegetation period. The $\Delta^{14}C$ generally gave higher values during summer and lower ones in wintertime. These values match the literature data and can be caused by agricultural and natural vegetation during the summer and weak vertical mixing, lack of CO_2 uptake during winter. The effects during winter can be caused by the lack of photosynthesis and the increased anthropogenic fossil emissions from regional and nearby settlements. In the case of the COVID-19 crisis in Hungary there were no significant changes in the trend of either CO_2 mole fraction or the $\Delta^{14}C$ results. The annual average fossil CO_2 excess values calculated at 115 m and 10 m altitude were 1.6 ppm and 1.9 ppm, respectively. Although higher values are observed at the lower measurement point (10 m), the overall average remains statistically similar. The first wave of COVID-19 in Hungary started on 11 March 2020, leading to the most stringent measures during the epidemic. The state of emergency was implemented until June. The analysis of the C_{foss} results for this period showed that the average concentrations in 2020 at both 115 m (1.03 ppm) and 10 m (1.6 ppm) altitude were not significantly different from the averages (1.23 and 1.42 ppm) of the previous five years. The observed seasonal variability, peaking in winter and reaching a trough in summer, is consistent with Major et al. 2018, suggesting that the excess is not solely attributable to local sources but represents a cumulative effect from a wider geographical area. To broaden our understanding of these effects in another environment, our team also sampled tree-rings from the Hungarian background station and from the two largest cities in Hungary (Budapest and Debrecen). The tree-ring analyses from Debrecen exhibit a good alignment with the regional background station, showing minimal deviations and negligible fossil loading both during the vegetation and first COVID-19 lockdown period. The result from Budapest revealed larger differences, by highlighting variations in fossil contributions at different measurement points. Results from tree-ring analyses presented that the effect of COVID-19 is not visible at all sites. It is possible that there are local effects, which may even show variations within urban areas. The use of our passive monitoring technique based on tree-ring data provides a valuable tool for investigating such differences.

Supplementary material. To view supplementary material for this article, please visit https://doi.org/10.1017/RDC.2024.133

Acknowledgments. Project NO. C2295145 has been implemented with the support provided by the Ministry of Culture and Innovation of Hungary from the National Research, Development and Innovation Fund, financed under the KDP 2023 ELTE funding scheme. The research at Isotoptech – Atomki AMS Laboratory was supported by the European Union and the State of

Hungary, co-financed by the European Regional Development Fund in the project of GINOP-2.3.4–15-2020–00007 "INTERACT". Fund and supported by the PARIS project (Grant Agreement No. 820846), which is funded by the European Commission through the Horizon Europe research programme. Supported by the ÚNKP-22-3 new National Excellence Program of Ministry for Culture and Innovation from the source of the National Research, Development and Innovation Fund. IM was supported by the Bolyai Scholarship of the Hungarian Academy of Sciences (BO/00710/23/10). The research was funded by the National Multidisciplinary Laboratory for Climate Change, RRF-2.3.1-21-2022-00014 project.

References

Ballantyne AP, Alden CB, Miller JB, Tans PP and White JWC (2012) Increase in observed net carbon dioxide uptake by land and oceans during the past 50 years. *Nature* **488**(7409), 70–72. https://doi.org/10.1038/nature11299.

Beramendi-Orosco LE, González-Hernández G, Cienfuegos E and Otero F (2023) Changes in fossil CO_2 emissions in Mexico City during the COVID-19 lockdown deduced from atmospheric radiocarbon concentration. *Radiocarbon* 1–11. doi: 10.1017/RDC.2023.76.

Burgess MG, Ritchie J, Shapland J and Pielke R (2021) IPCC baseline scenarios have over-projected CO_2 emissions and economic growth. *Environmental Research Letters* **16**(1), 014016.

Buzási A (2022) Comparative assessment of heatwave vulnerability factors for the districts of Budapest, Hungary. *Urban Climate* **42**, 101127.

Draxler RR and Hess GD (1998) An overview of the HYSPLIT_4 modelling system for trajectories, dispersion, and deposition. *Australian Meteorological Magazine* 295–308.

Friedlingstein P, O'Sullivan M, Jones MW et al. (2020) Global Carbon Budget 2020. *Earth System Science Data* **12**(4), 3269–3340.

Gloor M, Bakwin P, Hurst D, Lock L, Draxler R and Tans P (2001) What is the concentration footprint of a tall tower? *Journal of Geophysical Research: Atmospheres* **106**(D16), 17831–17840.

Graven HD, Guilderson TP and Keeling RF (2012) Observations of radiocarbon in CO_2 at La Jolla, California, USA 1992–2007: Analysis of the long-term trend. *Journal of Geophysical Research: Atmospheres* **117**(D2). doi: 10.1029/2011JD016533.

Hammer Ø, Harper DAT and Ryan PD (2001) PAST: Paleontological Statistics Software Package for Education and Data Analysis. *Palaeontologia Electronica.*

Hammer S, Friedrich R, Kromer B et al. (2017) Compatibility of atmospheric $^{14}CO_2$ measurements: Comparing the Heidelberg Low-Level Counting Facility to international accelerator mass spectrometry (AMS) laboratories. *Radiocarbon* **59**(3), 875–883.

Haszpra L, Barcza Z, Davis KJ and Tarczay K (2005) Long-term tall tower carbon dioxide flux monitoring over an area of mixed vegetation. *Agricultural and Forest Meteorology* **132**(1–2), 58–77.

Haszpra L, Barcza Z, Hidy D, Szilágyi I, Dlugokencky E and Tans P (2008) Trends and temporal variations of major greenhouse gases at a rural site in Central Europe. *Atmospheric Environment* **42**(38), 8707–8716.

Haszpra L, Ramonet M, Schmidt M et al. (2012) Variation of CO_2; mole fraction in the lower free troposphere, in the boundary layer and at the surface. *Atmospheric Chemistry and Physics* **12**(18), 8865–8875.

Heiskanen J, Brümmer C, Buchmann N et al. (2022) The Integrated Carbon Observation System in Europe. *Bulletin of the American Meteorological Society* **103**(3), E855–E872.

Hertelendi E and Csongor E (1983) Anthropogenic ^{14}C excess in the troposphere between 1951 and 1978 measured in tree rings. *Radiochemical and Radioanalytical Letters* **56**(2), 103–110.

Hungarian Central Statistical Office (2023) Turned out where, in what numbers, and under what conditions we live. KSH. Retrieved in 2023 from https://nepszamlalas2022.ksh.hu/en/news/turned-out-where-in-what-numbers-and-under-what-conditions-we-live.

Janovics R, Futó I and Molnár M (2018) Sealed tube combustion method with MnO_2 for AMS ^{14}C measurement. *Radiocarbon* **60**(5), 1347–1355.

Kertész Z, Aljboor S, Angyal A et al. (2024) Characterization of urban aerosol pollution before and during the COVID-19 crisis in a central-eastern European urban environment. *Atmospheric Environment* **318**, 120267.

Kontuľ I, Povinec PP, Richtáriková M, Svetlik I and Šivo A (2022) tree rings as archives of atmospheric pollution by fossil carbon dioxide in Bratislava. *Radiocarbon* **64**(6), 1577–1585.

Kovalcsik T, Boros L and Pál V (2021) A COVID-19-járvány első két hullámának területisége Közép-Európában. *Területi Statisztika* **61**(3), 263–290.

Le Quéré C, Jackson RB, Jones MW et al. (2020) Temporary reduction in daily global CO_2 emissions during the COVID-19 forced confinement. *Nature Climate Change* **10**(7), 647–653.

Lee S-H, Kong M-J, Lee S-G, Park S-H and Kim Y-S (2023) Recent spatial distribution of radiocarbon in urban tree leaves at Gyeongju, South Korea. *Radiocarbon* **65**(1), 201–207.

Levin I, Hammer S, Kromer B and Meinhardt F (2008) Radiocarbon observations in atmospheric CO_2: Determining fossil fuel CO_2 over Europe using Jungfraujoch observations as background. *Science of the Total Environment* **391**(2–3), 211–216.

Levin I, Kromer B and Hammer S (2013) Atmospheric $\Delta^{14}CO_2$; trend in Western European background air from 2000 to 2012. *Tellus B: Chemical and Physical Meteorology* **65**(1), 20092.

Levin I, Kromer B, Schmidt M and Sartorius H (2003) A novel approach for independent budgeting of fossil fuel CO_2 over Europe by $^{14}CO_2$ observations. *Geophysical Research Letters* **30**(23). doi: 10.1029/2003GL018477

Levin I, Naegler T, Kromer B et al. (2010) Observations and modelling of the global distribution and long-term trend of atmospheric $^{14}CO_2$. *Tellus B: Chemical and Physical Meteorology* **62**(1), 26.
Levin I, Schuchard J, Kromer B and Münnich KO (1989) The Continental European Suess Effect. *Radiocarbon* **31**(3), 431–440.
Liu Z, Ciais P, Deng Z et al. (2020) Near-real-time monitoring of global CO_2 emissions reveals the effects of the COVID-19 pandemic. *Nature Communications* **11**(1), 5172.
Major I, Haszpra L, Rinyu L, Futó I, Bihari Á, Hammer S, Jull AJT and Molnár M (2018) Temporal variation of atmospheric fossil and modern CO_2 excess at a Central European rural tower station between 2008 and 2014. *Radiocarbon* **60**(5), 1285–1299. https://doi.org/10.1017/rdc.2018.79.
Maxwell RS and Larsson L-A (2021) Measuring tree-ring widths using the CooRecorder software application. *Dendrochronologia* **67**, 125841.
Meijer HAJ, Smid HM, Perez E and Keizer MG (1996) Isotopic characterisation of anthropogenic CO_2 emissions using isotopic and radiocarbon analysis. *Physics and Chemistry of the Earth* **21**(5–6), 483–487.
Ministry of Agriculture, Nature and Food Quality of the Netherlands (2021) Hungary: Pandemic travel. Agroberichten Buitenland. Retrieved from https://www.agroberichtenbuitenland.nl/actueel/nieuws/2021/02/01/hungary-pandemic-travel.
Molnár M, Haszpra L, Svingor É, Major I and Svetlik I (2010a) Atmospheric fossil fuel CO_2 measurement using a field unit in a Central European City during the winter of 2008/09. *Radiocarbon* **52**(2), 835–845.
Molnár M, Major I, Haszpra L, Světlík I, Svingor É and Veres M (2010b) Fossil fuel CO_2 estimation by atmospheric ^{14}C measurement and CO_2 mixing ratios in the city of Debrecen, Hungary. *Journal of Radioanalytical and Nuclear Chemistry* **286**(2), 471–476.
Molnár M, Rinyu L, Veres M, Seiler M, Wacker L and Synal H-A (2013) EnvironMICADAS: A Mini ^{14}C AMS with Enhanced Gas Ion Source Interface in the Hertelendi Laboratory of Environmental Studies (HEKAL), Hungary. *Radiocarbon* **55**(2), 338–344.
Němec M, Wacker L, Hajdas I and Gäggeler H (2010) Alternative methods for cellulose preparation for AMS measurement. *Radiocarbon* **52**(3), 1358–1370.
Rinyu L, Molnár M, Major I et al. (2013) Optimization of sealed tube graphitization method for environmental ^{14}C studies using MICADAS. *Nuclear Instruments and Methods in Physics Research Section B: Beam Interactions with Materials and Atoms* **294**, 270–275.
Sharma R, Kunchala RK, Ojha S, Kumar P, Khandelwal D, Gargari S and Chopra S (2023) Spatial distribution of fossil fuel CO_2 in megacity Delhi determined using radiocarbon measurements in peepal (*ficus religiosa*) tree leaves. *Radiocarbon* **65**(4), 967–978. https://doi.org/10.1017/rdc.2023.66.
Stein AF, Draxler RR, Rolph GD, Stunder BJB, Cohen MD and Ngan F (2015) NOAA's HYSPLIT Atmospheric Transport and Dispersion Modeling System. *Bulletin of the American Meteorological Society* **96**(12), 2059–2077.
Stokes MA and Smiley TL (1968) *An Introduction to Tree-Ring Dating*. Chicago, IL.: University of Chicago Press.
Stuiver M and Polach HA. 1977. Discussion: Reporting of ^{14}C data. *Radiocarbon* **19**(3), 355–363.
Sturm P (2005) Atmospheric oxygen and associated tracers from flask sampling and continuous measurements: tools for studying the global carbon cycle. PhD thesis, University of Bern, Bern, Switzerland.
Svetlik I, Povinec PP, Molnár M et al. (2010) Estimation of long-term trends in the tropospheric $^{14}CO_2$ activity concentration. *Radiocarbon* **52**(2), 815–822.
Trumbore S (2009) Radiocarbon and soil carbon dynamics. *Annual Review of Earth and Planetary Sciences* **37**(1), 47–66.
Turnbull JC, Sweeney C, Karion A et al. (2015) Toward quantification and source sector identification of fossil fuel CO_2 emissions from an urban area: Results from the INFLUX experiment. *Journal of Geophysical Research: Atmospheres* **120**(1), 292–312.
Varga T, Barnucz P, Major I et al. (2019a) Fossil carbon load in urban vegetation for Debrecen, Hungary. *Radiocarbon* **61**(5), 1199–1210.
Varga T, Palcsu L, Ohta T, Mahara Y, Jull AJT and Molnár M (2019b) Variation of ^{14}C in Japanese Tree Rings Related to the Fukushima Nuclear Accident. *Radiocarbon* **61**(4). doi: 10.1017/RDC.2019.47.
Wacker L, Bonani G, Friedrich M et al. (2010) MICADAS: Routine and high-precision radiocarbon dating. *Radiocarbon* **52**(2), 252–262.
Zhou W, Niu Z, Wu S et al. (2022) Recent progress in atmospheric fossil fuel CO_2 trends traced by radiocarbon in China. *Radiocarbon* **64**(4), 793–803.
Zondervan A and Meijer HAJ (1996) Isotopic characterisation of CO_2; sources during regional pollution events using isotopic and radiocarbon analysis. *Tellus B: Chemical and Physical Meteorology* **48**(4), 601.

Cite this article: Baráth BÁ, Varga T, Major I, Haszpra L, Vargas D, Barcza Z, and Molnár M. Investigating the impact of COVID-19 on the atmospheric ^{14}C trend and fossil carbon load at urban and background sites in Hungary. *Radiocarbon*. https://doi.org/10.1017/RDC.2024.133